Modelling of ground-borne vibration when the train speed approaches the critical speed

J.Y. Shih[1], D.J. Thompson[1] and A. Zervos[2]

[1] Institute of Sound and Vibration Research, Faculty of Engineering and the Environment, University of Southampton, Southampton, SO17 1BJ, United Kingdom

Tel: +44 745 5857573, E-mail: js10e12@soton.ac.uk

[2] Infrastructure Research Group, Faculty of Engineering and the Environment, University of Southampton

Summary

When trains run on soft ground, large deflections of the track and vibration of the ground can occur when the train speed approaches the speed of Rayleigh waves in the ground. Modelling is helpful to understand and mitigate such critical velocity effects. Here, a three-dimensional time-domain model of a load moving on a track and ground has been developed in the finite element software ABAQUS. This allows nonlinear soil properties to be considered. In order to validate the approach, the vibration of the track and ground induced by a high speed train is compared with those from the site measurements carried out in the late 1990s at Ledsgård, Sweden. Due to the particularly soft soil at this site, it is necessary to adopt a nonlinear soil model due to the large deflections induced by the high-speed train. It is shown that using a linear model based on the small strain soil parameters leads to results which underestimate the displacements. Laboratory test data allow the nonlinear characteristics to be obtained. These have previously been used by various authors in an equivalent linear model. Here this approach is compared with a fully nonlinear model.

1 Introduction

Due to the demands of increasing population as well as environmental concerns, there is an urgent need for higher train speeds and increased capacity of the railways in many countries. As the train speed increases, however, track deflections can become larger. Particularly large displacements can occur when the speed of the train approaches the speed of waves in the ground and embankment, known as the critical velocity. These large displacements may lead to damage of the track components and may cause environmental impact for the neighbourhood. As a result, good design of high-speed railways depends on an accurate assessment of such critical velocity effects so that they can be avoided. In addition, better understanding of the stresses in the subgrade and the amplitudes of vibration of the whole system can lead to reductions in the cost of maintenance and an improvement in the quality of the railway system.

A number of theoretical models have been developed by various authors in an attempt to understand and predict such phenomena. Approaches adopted include semi-analytical models [1–4] and numerical models [5–11] based on finite element and boundary element approaches. Both frequency domain [1–4, 6, 8, 9] and time domain [5, 7, 10, 11] approaches have been considered. In predicting environmental ground vibration from trains, linear elastic models of the soil are normally used, which is generally justified by the fact that the strains are small. However, when the track deflections increase, as the train speed approaches the critical velocity, nonlinear effects may become important [2, 3, 6], especially in the region near the track. Of particular interest in this regard is the soft soil site at Ledsgård, south of Gothenburg in Sweden, where field tests were carried out in the late 1990s with trains running at or near the critical velocity [2, 3] as well as extensive soil investigations [5, 6].

According to laboratory tests, soil stiffness depends on cyclic strain amplitude, as well as a number of other factors such as mean principal effective stress, plasticity index, void ratio, over-consolidation ratio, and the number of loading cycles [12]. It is particularly important, in modelling nonlinear soil behaviour, especially at shear strains larger than $\sim 10^{-5}$ to 10^{-4}, to determine the dependence of the shear modulus on the strain [13]. With increased strain level, reductions in soil stiffness (stiffness degradation) and increases in damping ratio are obtained using cyclic triaxial tests [12, 14–16] and can be described by a shear modulus reduction curve and corresponding curve of damping ratio as a function of shear strain.

To include these effects in a model of the track and ground, several authors have used equivalent linear models[2, 3, 5, 6, 17]. An equivalent linear model involves an iterative procedure that can approximate nonlinear behaviour efficiently and can be more numerically stable than a fully nonlinear calculation. From an initial calculation, an 'effective' shear strain is determined from the time-varying strains. This is then used with the measured curves of shear modulus and damping at different shear strains to calculate updated values of the shear modulus and damping ratio applying to the motion. The model is run again until the strains obtained correspond to the assumed modulus. The effective shear strain used in this process is chosen as a proportion of the maximum strain in order to characterise the motion. From seismic tests a value of 0.65 times the maximum shear strain is used for this purpose [12]. In [2, 3, 5] such an equivalent linear model was used for the soft soil site of Ledsgård and good agreement was found with site measurements of track deflections. In these models, however, the stiffness reduction, based on an approximate effective strain level, was applied to all elements within a given soil layer. A more advanced approach was implemented by Costa et al. [6] in which the shear modulus was adjusted according to the maximum effective shear strain in each element of the 2D cross-section, resulting in a transverse inhomogeneity in the ground. It was found that a number of iterations were required to reach a value of shear modulus that was consistent with the corresponding strain level. This approach gave good agreement with the measurements.

The nonlinear stress-strain behaviour of soils can be represented more accurately by cyclic nonlinear constitutive models that follow the actual stress-strain path during cyclic loading. This behaviour can be characterized by a backbone curve and a series of rules that govern unloading-reloading behaviour, stiffness degradation, and other effects such as irregular loading, densification, pore pressure generation, etc. A popular cyclic model was given by Iwan [18] based on a series of parallel Jenkin elements, which consist of a linear spring in series with a frictional slider, to describe the backbone curve and the yield level. This model was adopted by Gomes Correia and Cunha [19] to study the effect of subgrade nonlinearity on the track response induced by a high-speed train. Such cyclic models can represent the development of permanent strains, hardening under drained conditions or stiffness degradation under undrained conditions due to pore pressure development. A more complex nonlinear model was used by Fernandes [20] to represent the ballast and soil nonlinearity beneath a railway track. The dynamic response after five cycles of loading due to moving axles was obtained and permanent displacements were modelled for understanding the behaviour of the soil and ballast degradation. However, the model is very complex and requires many parameters to construct the soil constitutive model.

A simpler nonlinear model is introduced here that is based on the shear modulus reduction curve. At each time step the soil stiffness in each element is determined based on the instantaneous octahedral shear strain. This is implemented in a user-defined subroutine within the software ABAQUS. Plastic behaviour is not considered here as it can be considered to be small compared with the transient dynamic deflections and the objective of the present work is not to study track settlement. Finally, the results are compared with site measurements from Ledsgård 6. The influence of the soil nonlinearity on the critical speed and stress-strain behaviour for the embankment and ground is investigated when the train speed approaches the critical speed.

2 Nonlinear soil model

During cyclic loading, the soil stress-strain behaviour typically follows a nonlinear hysteresis loop, as shown in Figure 1. The slope of the stress-strain curve can be identified as the soil stiffness; when it is loaded in shear this is the shear modulus. The dissipation energy, which is related to the damping ratio, can be determined from the area of the loop. The secant shear modulus is defined in terms of the maximum values of stress and strain as indicated in Figure 1. As the amplitude of the loading increases, it can be seen that this modulus reduces in the example shown, with the maximum shear modulus occurring for very small amplitudes. The ratio of the secant shear modulus at a given strain level to the maximum shear modulus can be identified as the shear modulus reduction associated with this amplitude. Figure 2(a) shows shear modulus reduction curves obtained from cyclic triaxial tests at different amplitudes, for material samples obtained at Ledsgård [6]. In contrast to the stiffness, the damping ratio tends to increase when the strain level increases, as shown in Figure 2(b).

A new material constitutive model has been developed in a user subroutine UMAT in the commercial finite element program, ABAQUS, based on shear modulus reduction curves such as these. This subroutine operates on each integration point by receiving variables such as the incremental strain vector and the previous stress vector, and returns the current stress vector and updated Jacobian matrix (current tangent modulus matrix). The new Young's modulus is obtained from the modulus reduction curve which is given in terms of the shear strain

value. However, due to the fact that a moving train induces a complex three-dimensional deflection which involves multiple strain components, the octahedral shear strain is used as the strain index to evaluate the value of modulus reduction for each time step. This is given by

$$\gamma_{oct} = \frac{1}{3}\sqrt{\left(\varepsilon_{xx}-\varepsilon_{yy}\right)^2+\left(\varepsilon_{yy}-\varepsilon_{zz}\right)^2+\left(\varepsilon_{xx}-\varepsilon_{zz}\right)^2+6\left(\gamma_{xy}^2+\gamma_{yz}^2+\gamma_{xz}^2\right)} \tag{2.1}$$

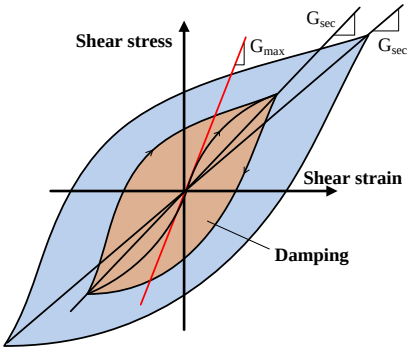

Figure 1 Shear stress-strain path during cyclic loading

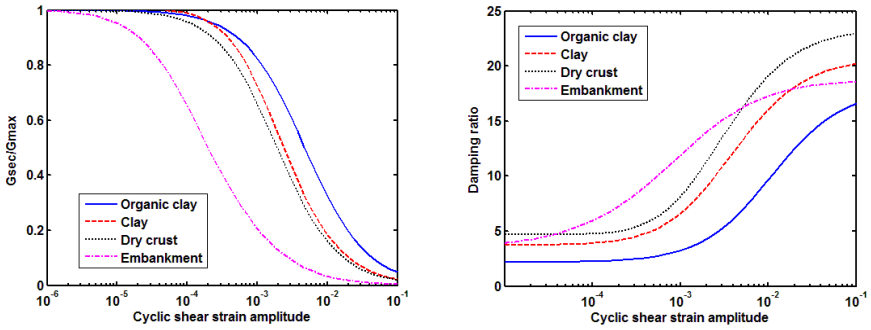

(a) **(b)**

Figure 2. Nonlinear soil characteristic from Ledsgård (a) shear modulus reduction curve; (b) damping ratio [6]

From the new Young's modulus, determined from the modulus reduction curve, the new constitutive matrix

$$[D]=\begin{bmatrix} \lambda+2\mu & \lambda & \lambda & 0 & 0 & 0 \\ \lambda & \lambda+2\mu & 0 & 0 & 0 & 0 \\ \lambda & \lambda & \lambda+2\mu & 0 & 0 & 0 \\ 0 & 0 & 0 & \mu & 0 & 0 \\ 0 & 0 & 0 & 0 & \mu & 0 \\ 0 & 0 & 0 & 0 & 0 & \mu \end{bmatrix} \tag{2.2}$$

is obtained, in which

$$\lambda=\frac{vE}{(1+v)(1-2v)};\quad \mu=\frac{E}{2(1+v)} \tag{2.3}$$

with E the Young's modulus and v the Poisson's ratio. The stress matrix is then updated for the next time step i+1 based on this new tangent constitutive matrix

$$\{\sigma\}_{i+1}=[D]_i\{\varepsilon\}_i \tag{2.4}$$

and the strain which is updated by the strain increment $d\varepsilon$

$$\{\varepsilon\}_i=\{\varepsilon\}_{i-1}+\{d\varepsilon\}_i \tag{2.5}$$

The stress and strain vectors are given by

$$\{\sigma\} = \{\sigma_{xx} \quad \sigma_{yy} \quad \sigma_{zz} \quad \tau_{xy} \quad \tau_{yz} \quad \tau_{xz}\}^T \tag{2.6}$$

$$\{\varepsilon\} = \{\varepsilon_{xx} \quad \varepsilon_{yy} \quad \varepsilon_{zz} \quad \gamma_{xy} \quad \gamma_{yz} \quad \gamma_{xz}\}^T \tag{2.7}$$

Changes to the damping ratio are not considered here. A constant damping ratio is used based on Rayleigh damping. In this approach the damping matrix is a proportional to the mass and stiffness matrices with the factors α and β as follows

$$[C] = \alpha[M] + \beta[K] \tag{2.8}$$

To determine α and β, two frequencies, ω_1 and ω_2, are chosen at which the target damping ratio ξ is to be matched. Then

$$\alpha = \frac{2\xi\omega_1\omega_2}{\omega_1 + \omega_2}, \qquad \beta = \frac{2\xi}{\omega_1 + \omega_2} \tag{2.9}$$

The mass-proportional component of damping can be incorporated directly in the ABAQUS FE code for built-in constitutive models and is assumed not to vary with strain level. However, for a user-defined material, the stiffness-proportional damping must be incorporated in the user-defined material subroutine, UMAT. This can be achieved by adding the corresponding stress term, where β is assumed constant:

$$\{\sigma_d\}_{i+1} = \beta[D]_i \{\dot{\varepsilon}\}_i \tag{2.10}$$

where $\dot{\varepsilon}$ is the strain rate, to the stress resulting from the elastic responses at each integration point. As a result, the total stress can be calculated by

$$\{\sigma_T\}_{i+1} = \{\sigma\}_{i+1} + \{\sigma_d\}_{i+1} \tag{2.11}$$

3 Numerical model

3.1 FE model

A three-dimensional FE model has been constructed of the track and ground at the site at Ledsgård. Soil properties are available from various in-situ tests, including cross-hole, SASW and SCPT tests [5, 6]. In addition to the embankment, three main soil layers were identified, referred to as dry crust, organic clay, and clay. Measured shear wave speeds as a function of depth are shown in Figure 3(a) along with the values assumed here. The lower clay layer is assigned a shear wave speed that varies with depth. The material properties used for the various layers are listed in Table 1.

The FE mesh is shown in Figure 3(b). Use is made of symmetry about the track centreline. It has been found that, provided that the model is large enough, there is no benefit in using absorbing elements at the boundaries [21]. A cuboid model with fixed boundaries with a width of 40.5 m and a depth of 33.2 m is used. A damping model with a sufficiently large mass-proportional term should be used, allowing the energy to be dissipated sufficiently to avoid the reflections interrupting the results [21]. The target damping ratios for the four different materials are listed in Table 1. Rayleigh damping coefficients are obtained from Eq. (2.10) for target frequencies of 3 and 20 Hz. The length of the model required to achieve steady state depends on the load speed [21], with longer models required if the load speed approaches or exceeds the critical speed. Here, an 80 m long model is used which is found to be sufficient for convergence.

Table 1 Embankment/ground properties

	Thickness	P-wave speed	S-wave speed	Density	Damping ratio
Embankment	1.4 m	470 m/s	250 m/s	1800 kg/m^3	12%
Crust	1.1 m	500 m/s	60 m/s	1500 kg/m^3	7%
Organic clay	3.0 m	500 m/s	42 m/s	1250 kg/m^3	4%
Clay	29.1 m	1500 m/s	50~122.9 m/s	1470 kg/m^3	7%

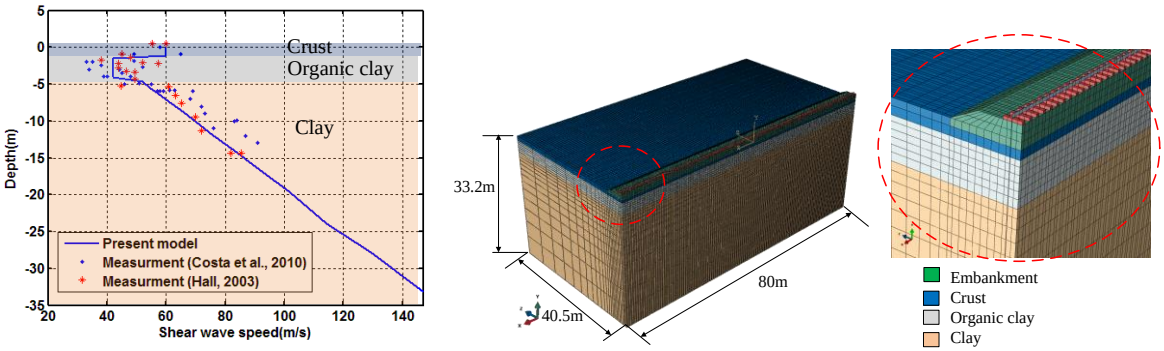

(a) **(b)**

Figure 3 Soil and railway embankment geometry and shear wave speed at Ledsgård based on soil investigations; (a) shear wave speed profile; (b) three-dimensional track/ground FE model

Fully-integrated quadratic cuboid elements are used for the whole ground model. Linear Timoshenko beam elements are used for the rail. To represent the railpads linear springs with stiffness $4.7\text{x}10^8$ N/m are used to connect the rail to each sleeper. Discrete sleepers with a spacing of 0.67 m are considered. The half-sleeper length, height, mass density, Young's modulus and Poisson's ratio are 1.3 m, 0.2 m, 2500 kg/m^3, 3×10^{10} N/m^2 and 0.15, respectively. The ballast is included in the embankment layer and this in turn is embedded to a depth of 0.4 m into the upper ground layer. The smallest element size is set to be 0.5 m in the vicinity of the track, which is sufficient for accurate modelling of local deflections up to around 50 Hz. However, the element size is increased gradually with a stretch factor of 1.2 in both the vertical and horizontal directions, as shown in Figure 3(b). This prevents the mesh size becoming too large and has been shown to be acceptable provided that far field wave propagation does not occur. The total number of degrees of freedom is 1.76 million.

3.2 Results for moving loads

Results are presented for moving axle loads, i.e. neglecting surface roughness excitation. Details of the train, X2000, are available from the literature [6]. Multiple loads are applied on the rail at the locations of the various axles and these are moved along the track according to the train speed. For the northbound train, with the locomotive leading, only two vehicles (eight axles) are considered, because the maximum deflections occurred for the front vehicle. However, the full train set is considered for analysis of the southbound direction. For linear analysis a single moving load is used with superposition to determine the response to the whole train.

The parameters for the organic clay are the most important for the behaviour of the whole system as this is the softest layer, see Table 1. Measurement data for this material, obtained from triaxial tests [6], is shown in Figure 4(a) in the form of the shear modulus reduction. Two fitted lines are given which are used in the material constitutive model described in Section 2 to represent the soil nonlinearity. These two nonlinear models as well as a linear model based on the unreduced parameters in Table 1, are compared with the measurements. Results for a train speed of 50 m/s are shown in Figure 4(b). Good agreement with the measurements is found by using the second nonlinear model, which is slightly stiffer than the first one. The peak deflection from the first nonlinear model is almost double that from the second one. On the other hand, the results from the linear model tend to be too small compared with the measurement.

The maximum upward and downward displacements for different train speeds are shown in Figure 5(a). Results are shown from the site measurements, the linear model and the second nonlinear model. The critical speed, at which the maximum deflection occurs, is found at around 55~60m/s. A similar value is also found in the literature [2, 3, 6]. Good agreement is found with the nonlinear model. The maximum displacement at the critical speed, at around 15 mm, is roughly double the result due to the static load. On the other hand, the linear model predicts a critical speed of around 70 m/s, which is ~15% higher than the results from the nonlinear model. Furthermore, the maximum deflections close to the critical speed are much smaller than for the nonlinear model. It is clear that soil nonlinearity should be considered for this site at the higher train speeds, although the results from the linear model agree reasonably well with the measurement for speeds lower than 40 m/s.

Figure 5(b) shows the maximum octahedral shear strains at different depths within the organic clay layer obtained from the nonlinear model for different train speeds. The strain level increases significantly when the load speeds are higher than around 45 m/s. Furthermore, the strain level at higher speeds is around three times

larger than the results at low speed. Comparing these values with the modulus reductions curves in Figure 4(a) it can be seen that the modulus will be reduced to between 90% and 70% of the small strain stiffness (according to model 2).

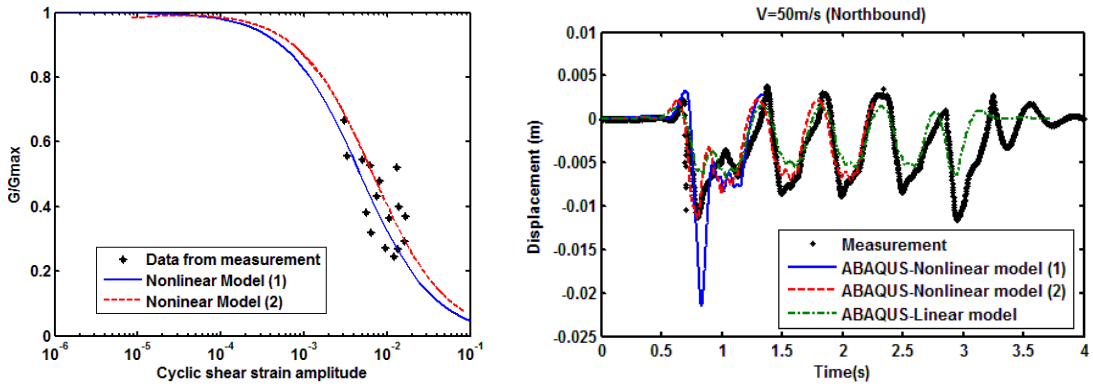

(a) (b)

Figure 4 Nonlinear model; (a) shear modulus reduction curve for organic clay layer; (b) displacement comparison between linear, nonlinear models and measurement for load speed 50m/s (northbound)

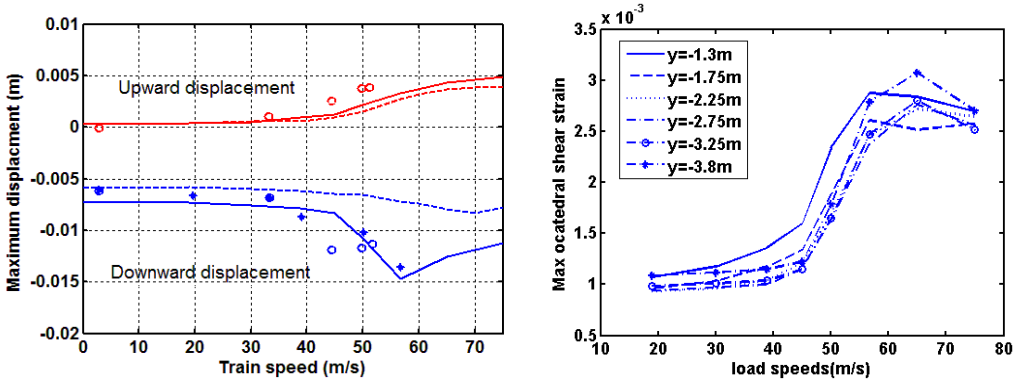

(a) (b)

Figure 5 Assessment of critical speed; (a) displacement -: nonlinear model; --: linear model; o: northbound measurement data; *: southbound measurement data; (b) maximum octahedral strain level for organic clay layer at different load speed

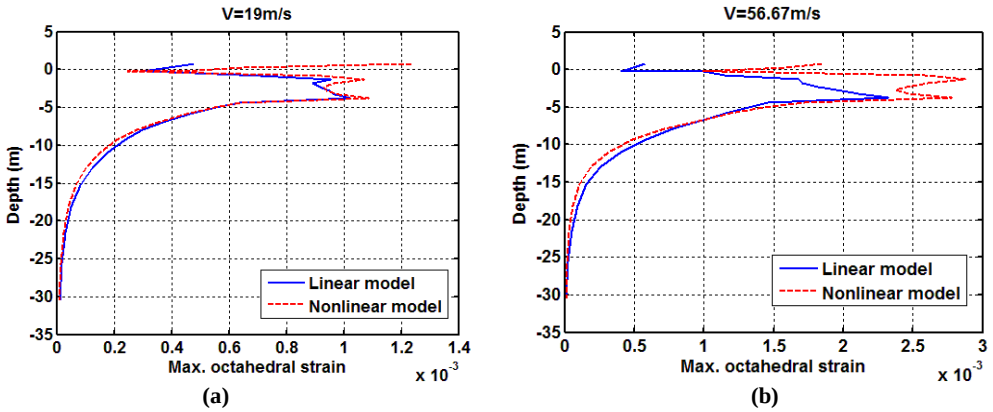

(a) (b)

Figure 6 Maximum octahedral shear strain against depth from northbound analysis for two different load speeds; (a) 19m/s; (b) 56.7m/s

The maximum octahedral shear strains are shown in Figure 6 as a function of the depth for two different train speeds. Results are shown for linear and nonlinear models. As can be seen, the strain levels are typically 10^{-3} which is too large to allow use of the small strain approximation (see Figure 4(a)). Nevertheless, for the load speed of 19 m/s, the results of the linear and nonlinear models are very similar, except at the embankment.

Figure 7(a) compares the track deflections under the train with measurements, showing good agreement even for the linear model. In contrast, as shown in Figure 7(b), for a train speed of 56.7 m/s the results from the linear model are around 40% smaller than the measurements whereas the nonlinear model gives good agreement. Figure 6(b) shows that the strain level in the organic clay layer is around 30% higher for the nonlinear model than the linear model.

Finally, the octahedral shear strain at the top surface of the organic clay layer for a load speed at 56.67m/s is shown in Fig. 8. The strain level from nonlinear model is not only larger than the result from the linear model but the shape of the propagation is different. A clear wave shaped pattern occurs for the nonlinear model. This is because the load speed is higher than the wave speed in the ground, whereas for the linear model it is still below the critical speed. Furthermore, even though the strain level decreases significantly away from the track, octahedral shear strains of around 10^{-3} still can be found at 30 m away from the track for the nonlinear model, as shown in Fig. 8(b).

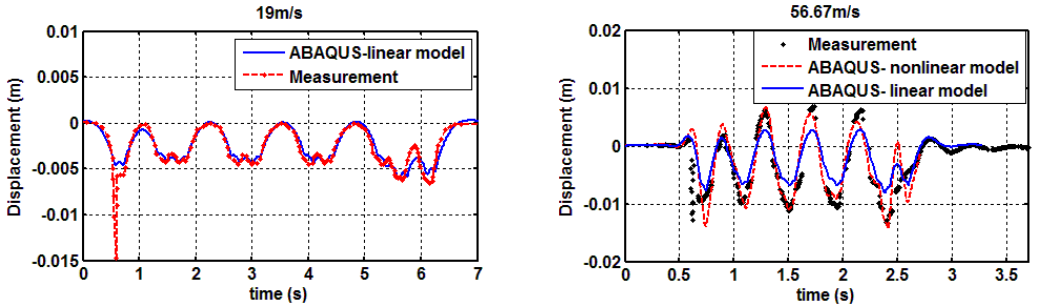

(a) **(b)**

Figure 7 Displacements for southbound train for two different speeds; (a) 19m/s; (b) 56.7m/s

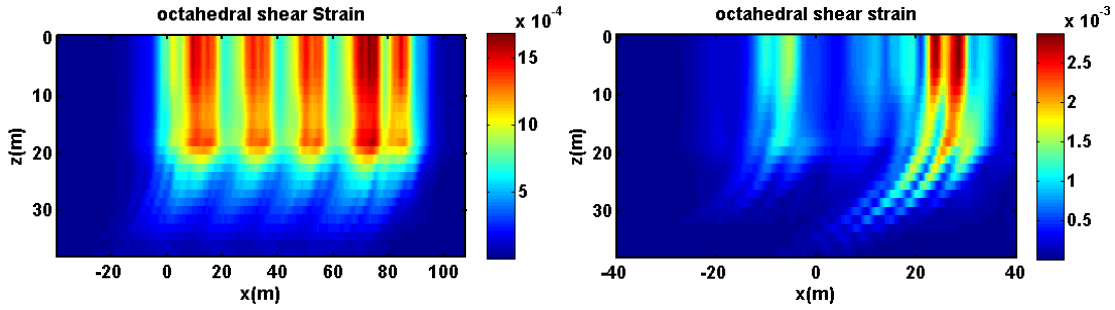

(a) **(b)**

Figure 8 Octahedral shear strain from linear and nonlinear model at load speed 56.67m/s (Northbound); (a) linear model; (b) nonlinear model

4 Conclusions

A three-dimensional vehicle/track/ground model that includes soil nonlinearity has been developed that operates in the time domain. Soil nonlinearity has been implemented within the FE model in terms of shear modulus degradation. Good agreement has been found compared to site measurements at the soft soil site in Ledsgård, Sweden. The effect of soil nonlinearity becomes significant at this site when the load speeds approach or exceed the critical speed. The maximum track displacements for load speeds close to the critical speed are around twice those found at lower speeds. The maximum strain levels in the subgrade increase by around a factor of three.

The critical speed obtained from the linear model is higher than that obtained from the nonlinear model. The displacements from the linear model are underestimated, especially for speeds approaching the critical speed. Nevertheless, good agreement is found for lower speeds. Two different shear modulus reduction curves have been considered here in the nonlinear model, both of which are consistent with soil data obtained in triaxial tests. The results are found to be very sensitive to the choice of this curve.

Acknowledgements

The work described has been supported by the EPSRC under the Programme Grant EP/H044949/1, 'Railway Track for the 21st Century'.

References

1. Sheng, X., Jones, C. J. C. & Petyt, M. Ground vibration generated by harmonic load acting on a railway track. J. Sound Vib. **225,** 3–28 (1999).
2. Kaynia, A. M., Madshus, C. & Zackrisson, P. Ground vibration from high-speed trains: prediction and countermeasure. J. Geotech. Geoenvironmental Eng. **126,** 531–537 (2000).
3. Madshus, C. & Kaynia, A. M. High-speed railway lines on soft ground: dynamic behaviour at critical train speed. J. Sound Vib. **231,** 689–701 (2000).
4. Krylov, V. V. Generation of ground vibrations by superfast trains. Appl. Acoust. **44,** 149–164 (1995).
5. Hall, L. Simulations and analyses of train-induced ground vibrations in finite element models. Soil Dyn. Earthq. Eng. **23,** 403–413 (2003).
6. Costa, P. A., Calçada, R., Cardoso, A. S. & Bodare, A. Influence of soil non-linearity on the dynamic response of high-speed railway tracks. Soil Dyn. Earthq. Eng. **30,** 221–235 (2010).
7. El Kacimi, A., Woodward, P. K., Laghrouche, O. & Medero, G. Time domain 3D finite element modelling of train-induced vibration at high speed. Comput. Struct. **118,** 66–73 (2013).
8. Sheng, X., Jones, C. J. C. & Thompson, D. J. Modelling ground vibration from railways using wavenumber finite- and boundary-element methods. Proc. R. Soc. A Math. Phys. Eng. Sci. **461,** 2043–2070 (2005).
9. Yang, Y. B., Hung, H. H. & Chang, D. W. Train-induced wave propagation in layered soils using finite/infinite element simulation. Soil Dyn. Earthq. Eng. **23,** 263–278 (2003).
10. Kouroussis, G., Verlinden, O. & Conti, C. Ground propagation of vibrations from railway vehicles using a finite/infinite-element model of the soil. Proc. Inst. Mech. Eng. Part F J. Rail Rapid Transit **223,** 405–413 (2009).
11. Shih, J. Y., Thompson, D. & Zervos, A. Assessment of track-ground coupled vibration induced by high-speed trains. in 21st Int. Congr. Sound Vib. 13–17 (2014).
12. Kramer, S. L. Geotechnical Earthquake Engineering. (Prentice-Hall, Inc., 1996).
13. Beresnev, I. A. & Wen, K. Nonlinear soil response a reality ? Bull. Seismol. Soc. Am. **86,** 1964–1978 (1996).
14. Ishibashi, I. & Zhang, X. Unified dynamic shear moduli and damping ratio of sand and clay. Soils Found. **33,** 182–191 (1993).
15. Iwasaki, T., Tatsuoka, F. & Takagi, Y. Shear moduli of sand under cyclic torsional shear loading. Soils Found. **18,** 39–56 (1978).
16. Kokusho, T. Cyclic triaxial test of dynamic soil properties for wide strain range. Soils Found. **20,** 45–60 (1980).
17. Thach, P.-N., Liu, H.-L. & Kong, G.-Q. Vibration analysis of pile-supported embankments under high-speed train passage. Soil Dyn. Earthq. Eng. **55,** 92–99 (2013).
18. Iwan, W. D. On a class of models for the yielding behavior of continuous and composite systems. J. Appl. Mech. **34,** 612–617 (1967).
19. Gomes Correia, A. & Cunha, J. Analysis of nonlinear soil modelling in the subgrade and rail track responses under HST. Transp. Geotech. **1,** 147–156 (2014).
20. Fernandes, V. A. Suject: numerical analyis of nonlinear soil behavior and heterogeneity effects on railway track response. (2014).
21. Shih, J. Y., Thompson, D. J. & Zervos, A. Modelling scheme for railway vehicle/track/ground dynamic interaction in the time domain. in Proc. 24th UK Conf. Assoc. Comput. Mech. Eng. (2016).